This is a repository copy of *Comparison of flux-weakening control strategies of novel hybrid-excited doubly salient synchronous machines*.

Comparison of Flux-weakening Control Strategies of Novel Hybrid-excited Doubly Salient Synchronous Machines

N. Pothi, Z. Q. Zhu, and Y. Ren

⊕*Abstract* -- **For hybrid-excited doubly salient synchronous machine, both the field excitation current and the d-axis current can be utilized to adjust the flux-linkage, which provides more flexible control parameters for flux-weakening operation. In this paper, three flux-weakening control methods, i.e. utilizing field excitation current alone (Method-I), utilizing armature current alone (Method-II), and optimal method (Method-III), are proposed and compared. All three methods can achieve similar torque performance in the constant-torque region. In the flux-weakening region, Method-I exhibits low torque and limited operating range. The operating speed range can be further extended by Method-II and Method-III. In addition, Method-III can provide a higher efficiency in flux-weakening region than Method-II since the copper loss of field winding can be decreased in proportion to the reduction of field excitation current. Those flux-weakening control methods are verified by experimental results.**

Index Terms—**Efficiency improvement, flux-weakening, hybrid-excited, optimal.**

NOMENCLATURE

i_d, i_q	d- and q-axis currents
i_{dm}^*, i_{qm}^*	d-axis and q-axis modified reference currents
i_f	Field excitation current
$i_{f,\max}$	Maximum field excitation current
L_d, L_q, L_{mf}	d-axis, q-axis and mutual inductances
R_f, R_s	Field winding and armature resistances
v_α, v_β	α- and β-axis voltages
v_d, v_q	d- and q-axis voltages
v_{d_ff}, v_{q_ff}	d- and q-axis decoupling voltages
v_{dm}, v_{qm}	d- and q-axis output voltages of over-modulation block
T_e	Electromagnetic torque
T_s	Sampling period
Ψ_{pm}	Permanent magnet flux-linkage
θ	Electrical angular position of rotor
ω	Electrical rotor speed
ω_r	Mechanical rotor speed

I. INTRODUCTION

PERMANENT magnet synchronous machines (PMSMs) have been widely employed in many applications due to their advantages including high torque density, wide operating speed range, and high efficiency. For PMSMs, high speed operation above the base speed is realized by utilizing flux weakening control to suppress the back-EMF produced by permanent magnets (PMs). However, since only the PM is used as an excitation source for such machines, the viable control for improving efficiency is limited, as introduced in [1]. The searching efficiency improvement is proposed in which the d-axis current can be adjusted to track the optimal efficiency [2]. However, the current oscillation cannot be avoided and a slow dynamic response occurs due to intensive calculation [3].

Hybrid-excited doubly salient synchronous machine (HEDSSM), as shown in Fig. 1, which consists of two excitation sources, i.e. permanent magnets (PMs) and field windings, provide an extra flexibility to adjust the flux-linkage thanks to the existence of field excitation current. Therefore, higher torque at low speed and wider operating speed range, as well as higher efficiency over wider operation region can be provided [4]-[8]. Moreover, due to the fact that all the PMs and windings, i.e. field and armature windings, are located on the stator, HEDSSMs have robust rotor structure and excellent cooling capability [4]-[11].

According to the operating principle of the HEDSSM, the field excitation current is the major excitation source compared with the PMs. Therefore, the maximum field excitation current is commonly employed to achieve the highest torque [12]. However, in flux-weakening operation, the d-axis current is required to oppose the direction of field excitation flux produced by field excitation current. As a result, the efficiency in this region would be deteriorated due to the excessive copper loss of field winding. For HEDSSM, the field excitation current can also be utilized to weaken the flux-linkage. In [13], a specific value of field excitation current is utilized in flux-weakening region. However, a large torque drop is noticeable when the machine speed exceeds its rated speed. The methods based on Extended Lagrange multipliers optimization have been investigated in [13]-[14], where the optimal currents can be determined by the analytical expressions. However, they are sensitive to the variation of the machine parameters, and are difficult to implement due to high computational burden. Another flux-weakening control method of the HEDSSM is presented in [16], where the field excitation current and the d-axis current can be automatically adjusted depending on the operation regions. Although the influence of machine parameter variation can be avoided, the optimization of weakening currents, i.e. field excitation and d-axis currents, relating to the efficiency improvement in flux-weakening region is not considered.

Since there are two currents in the HEDSSM which can be utilized to weaken the flux-linkage, i.e. field excitation current and d-axis armature current, three flux-weakening

Nattapong Pothi was with the Department of Electronic and Electrical engineering, The University of Sheffield, UK, and is now with School of Engineering, University of Phayao, Phayao, Thailand (e-mail: nattapong.po@up.ac.th).

Z. Q. Zhu and Yuan Ren are with the Department of Electronic and Electrical engineering, The University of Sheffield, UK. (e-mail: z.q.zhu@sheffield.ac.uk, y.ren@sheffield.ac.uk).

control methods are proposed and compared in this paper: (1) utilizing field excitation current only (Method-I), (2) utilizing armature current only Method-II, and (3) optimal method which utilizes both the field excitation current and armature current (Method-III). In Method-I and Method-II, the weakening currents, i.e. field excitation and d-axis currents, are modified based on the voltage error regulation method [17]. In Method-III, the maximum efficiency condition is analyzed based on the differentiation of the efficiency with respect to the amplitude of armature current in order to determine the optimal field excitation current. All flux-weakening control methods are validated by experimental results.

II. Hybrid-excited Permanent Magnet Machine and Flux-weakening Control Method

In this section, the novel fault-tolerant prototype hybrid-excited machine and three flux-weakening control methods, which are classified based on the utilization of weakening currents, i.e. utilizing field excitation current only, utilizing armature current only, and optimal method, will be explained.

A. Fault-tolerant Hybrid-excited Permanent Magnet Machine

Fig. 1 shows the simplified structure of prototype HEDSSM which consists of 12-stator/10-rotor poles. In this topology, four armature coils in each phase (A, B, and C) and twelve field coils are separately connected in series, and those coils are wound on each of the stator poles. The slot openings between two stator poles are replaced by the PMs. Since there is no magnet or excitation coils on the rotor, the rotor structure is simple. The phase flux-linkage and back-emf waveforms for a specific field excitation current obtained by 2D finite element (FE) analysis are shown in Fig. 2. Since the phase flux-linkage is generated by both PM and field excitation current, the phase flux-linkage and back-emf can be efficiently adjusted by changing the value of field excitation current, as shown in Fig. 2(a) and (b) respectively. The novel feature of this HEDSSM is that when there is no field excitation current, the PM flux will be short-circuited via the stator teeth and the back iron, and thus, the open-circuit voltage of the windings will be zero and there is no over-voltage risk under uncontrolled generator fault at high speed operation. The operating principle and parameters of the prototype machine have been presented in [4].
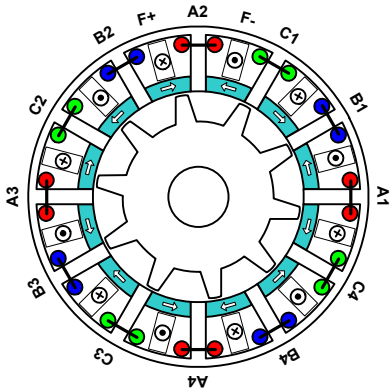
Fig. 1. Cross-section of the prototype HEDSSM.

(a) flux-linkage
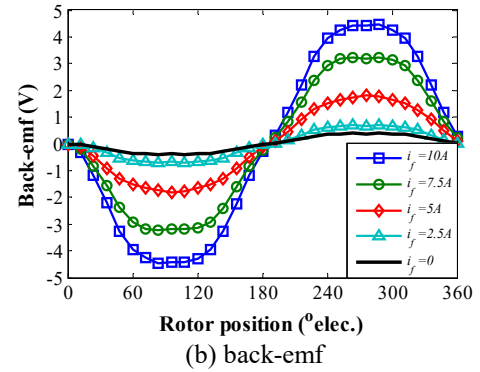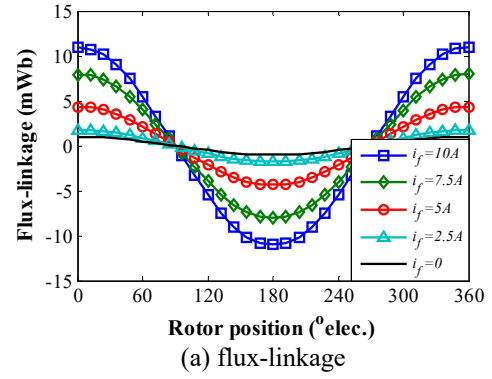
(b) back-emf

Fig. 2. Flux-linkage and back-emf adjustable capability.

(a) PM-flux $(i_{fs}^r = 0)$

(b) field excitation flux $(i_{fs}^r > 0)$

(c) Net enhancing flux-linkage

Fig.3. Flux-linkage adjustability of the prototype HEDSSM.

Fig. 3 shows the flux-linkage adjustability of the prototype machine. On open circuit ($i_{fs}^r = 0$), see Fig. 3(a), the PM-flux is inherently short-circuited via the stator back-iron without the flux linkage with the rotor. It is noted that under open-circuit condition, almost all of magnet flux is leakage flux, and that without the flux linkage with the rotor, there is no variation in stator flux-linkage as the rotor rotates, resulting in very low open-circuit back-emf regardless of speed, as shown in Fig. 2 (b). If only positive field excitation current ($i_{fs}^r > 0$) is applied without the consideration of the PM, as shown in Fig.3(b), the flux-linkage can be enhanced which is in the opposite direction of the short-circuited PM-flux. Therefore, by considering both flux sources, i.e. the PM and field winding, a net enhanced flux-linkage can be observed, Fig. 3(c). It can be seen from Fig. 3 that when the field excitation current is further increased, the PM flux is pushed into the air-gap.

B. Machine Model

The d-axis and q-axis voltages of the HEDSSM expressed in the synchronous reference frame are given by (1) and (2).

$$v_d = R_s i_d + L_d \frac{di_d}{dt} + L_{mf} \frac{di_f}{dt} - \omega L_q i_q \qquad (1)$$

$$v_q = R_s i_q + L_q \frac{di_q}{dt} + \omega \left(\psi_{pm} + L_d i_d + L_{mf} i_f \right) \qquad (2)$$

Since the flux-linkage of the d-axis and q-axis are given as $\psi_{pm} = \psi_{pm} + L_d i_d + L_{mf} i_f$ and $\psi_q = L_q i_q$, the electromagnetic torque (T_e) in steady-state condition is given by (3).

$$T_e = \frac{3}{2} P \left[\left(\psi_{pm} + L_{mf} i_f \right) i_q + \left(L_d - L_q \right) i_d i_q \right]. \qquad (3)$$

where P is the number of pole pairs.

Based on the unity saliency of the prototype machine [13] in which the d-axis and q-axis inductances are approximately equal, the torque equation can be expressed by (4).

$$T_e = \frac{3}{2} P \left(\psi_{pm} + L_{mf} i_f \right) i_q. \qquad (4)$$

C. Flux-weakening Control Method Utilizing Field Excitation Current (Method-I)

For HEDSSM, the flux-linkage can be effectively enhanced/weakened via field winding. Therefore, it is possible to adjust the field excitation current to extend the operating speed range in flux-weakening region. The flux-weakening control strategy utilizing field excitation current (Method-I) is illustrated in Fig. 4. The maximum field excitation current is initially employed to enhance the maximum torque in constant-torque region, and then it is adjusted in flux-weakening region by the modified field excitation current (Δ_f) as given by (5), which considers the difference between input voltages and the output voltages of the over-modulation block [17].

$$\Delta_f = \alpha \sqrt{ \frac{\omega_c}{s + \omega_c} (v_d^* - v_{dm}^*)^2 + \frac{\omega_c}{s + \omega_c} (v_q^* - v_{qm}^*)^2 } \qquad (5)$$

where α is the constant gain, ω_c is the bandwidth of the

low-pass filter (LPF), s is the integral operator, * denotes the reference value, v_f is the field excitation voltage.

All reference currents are shown in Table I, in which the maximum q-axis current can be maintained at the maximum armature current (I_m) in the whole operating speed range due to zero d-axis current.

Fig.4. Flux-weakening control strategy utilizing field excitation current (Method-I).

TABLE I
OPERATING CONDITIONS WITH UTILIZING FIELD EXCITATION CURRENT.

Reference currents	Constant-torque region	Flux-weakening region
i_d^*	0	
i_q^*	$\min \left(i_q^*, I_m \right)$	
i_f^*	$i_{f,max}$	$i_{f,max} - \Delta_f$

It should be noted that the HEDSSM's torque equation is a function of both the field excitation flux ($L_{mf}i_f$) and the q-axis current as given by (4), which is different from the conventional machine. Therefore, in Method-I, the torque generation in the flux-weakening region would be gradually decreased in proportion to the decreasing of field excitation current.

D. Flux-weakening Control Method Utilizing Armature Current (Method-II)

Fig. 5 shows the flux-weakening control of the HEDSSM based on the utilization of armature current as mentioned in [18]-[19], while the field excitation current is maintained at its maximum value in the whole operating speed range in order to achieve the maximum enhanced torque. Hence, only the d-axis armature current is utilized to weaken the flux-linkage when the voltage and current are beyond the predefined constraints, and the q-axis current reference needs to be modified accordingly. All reference currents are expressed in Table II.

1) Modification of the d-axis reference current

It is well known that for extending a speed range under the current and voltage limits, the d-axis reference current needs to be adjusted to weaken the flux-linkage. In this method, the modified d-axis current (Δ_d) is given by (6) [17]-[18]. It is also based on the voltage error regulation method, which has been explained in (1).

$$\Delta_d = \alpha \sqrt{ \frac{\omega_c}{s + \omega_c} (v_d^* - v_{dm}^*)^2 + \frac{\omega_c}{s + \omega_c} (v_q^* - v_{qm}^*)^2 }. \qquad (6)$$
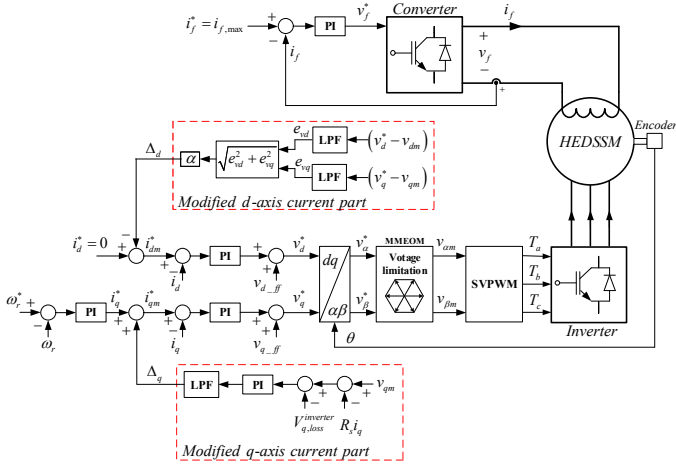
Fig.5. Flux-weakening control strategy utilizing armature current (Method-II).

TABLE II
OPERATING CONDITIONS WITH UTILIZING ARMATURE CURRENT.

REFERENCE CURRENTS	Constant-torque region	Flux-weakening region
i_{dm}^*	0	$i_d^* - \Delta_d$
i_{qm}^*	$\min\left(i_q^*, I_m\right)$	$\min\left(i_q^*, \sqrt{I_m^2 - i_d^2}\right) + \Delta_q$
i_f^*	$i_{f,\max}$	

Therefore, the modified d-axis reference current is given as,

$$i_{dm}^* = i_d^* - \Delta_d. \tag{7}$$

2) Modification of the q-axis reference current

When the machine operates under the infinite constant power speed ratio characteristic with $L_d I_m > \psi_{pm}$ [18]-[19] in which the q-axis voltage is controlled toward zero by the d-axis current, and hence, the higher speed range cannot be achieved. Under this condition, the q-axis current should be modified to track the maximum torque per voltage (MTPV) trajectory, which means the d-axis voltage will be controlled while the q-axis voltage is still maintained at zero. The modified q-axis current (Δ_q) is given by (8) as introduced in [18].

$$\Delta_q = \min\left(0, \left(k_p + \frac{k_i}{s}\right) \times \frac{\omega_c}{s + \omega_c}\left(v_q^* - v_{q,loss}^{inverter} - R_s i_q\right)\right) \tag{8}$$

where $v_{q,loss}^{inverter}$ is the estimated q-axis voltage loss of inverter. Consequently, the modified q-axis reference current can be given as,

$$i_{qm}^* = \min\left(i_q^*, \sqrt{I_m^2 - i_d^2}\right) + \Delta_q \tag{9}$$

The estimated voltage loss of inverter has been analyzed in [18]. It is determined by utilizing the ideal characteristic of switching power devices provided by the manufacturers, the dead time, and the measured dc-link voltage. The static gain of voltage loss (A_p), which is defined in literature as the intermediate parameter, is given as,

$$A_P = \frac{\left(V_{dc} - V_{ce} + V_d\right)\left(t_d + t_{on} - t_{off}\right)}{3T_s} + \frac{V_{ceo} + V_{do}}{6} \tag{10}$$

where V_{dc} is the measured dc-link voltage, V_{ce} and V_d are the voltages drop of switching power devices, t_d is the dead time,

t_{on} and t_{off} are the total turn-on and turn-off transition times, V_{ceo} and V_{do} are the threshold voltages of switching power devices. Based on the Park's transformation, the estimated q-axis voltage loss of inverter can be given by (11).

$$v_{q,loss}^{inverter} = -2A_P\left(sign(i_a)\sin\theta + sign(i_b)\sin\left(\theta - \frac{2\pi}{3}\right)\right. \\ \left. + sign(i_c)\sin\left(\theta + \frac{2\pi}{3}\right)\right) + \frac{r_{ce} + r_d}{2}i_q \tag{11}$$

where $i_{a,b,c}$ denote the phase currents, $sign$ is the signum function to define the current direction, and r_{ce} and r_d are the resistances of switching power devices.

E. Optimal Flux-weakening Control Method (Method-III)

As mentioned above, the maximum field excitation current is used for all operating regions in Method-II, which might cause a low efficiency in the flux-weakening region due to a redundant copper loss of field winding. Therefore, in order to achieve the higher efficiency of the HEDSSM, both the armature and field excitation currents will be utilized in Method III, where the reference values of i_d and i_q are the same as Method II, while the reference value of field excitation current is determined based on i_d and i_q to achieve optimal efficiency.

To simplify the calculation, an assumption is made to achieve the optimal efficiency: only the copper loss will influence the HEDSSM's efficiency, while the changes in other losses such as iron losses, magnet losses and mechanical loss can be neglected. Therefore, based on the utilization of the mechanical output power (P_m) and the electrical input power (P_e), accounting for the power consumption of the field winding, the HEDSSM's efficiency can be expressed by (12).

$$\eta = \frac{P_m}{P_e} = \frac{\left(\psi_{pm} + L_{mf}i_f\right)i_q\omega}{\left(R_s i_d^2 + R_s i_q^2 + \frac{2}{3}R_f i_f^2\right) + \left(\psi_{pm} + L_{mf}i_f\right)i_q\omega} \tag{12}$$

It should be noted that the factor of 2/3 for the field winding copper loss is a result of abc to dq-axis transformation. The d-axis and q-axis currents are expressed by amplitude (I) and angle (θ_i) of the armature current within the current limit in all operating regions. The maximum efficiency condition is determined based on the differentiation of the efficiency with respect to the amplitude of armature current as follows,

$$\frac{\partial \eta}{\partial I} = 0, \text{ where } I = \sqrt{i_d^2 + i_q^2}, \ (i_d = I\sin\theta_i, \ i_q = I\cos\theta_i)$$

$$\frac{\left(-R_s I^2 + \frac{2}{3}R_f i_f^2\right)\left(\psi_{pm} + L_{mf}i_f\right)\omega\cos\theta_i}{\left(R_s I^2 + \frac{2}{3}R_f i_f^2 + \left(\psi_{pm} + L_{mf}i_f\right)\omega I\cos\theta_i\right)^2} = 0 \tag{13}$$

Thus,

$$\left(-R_s I^2 + \frac{2}{3}R_f i_f^2\right)\left(\psi_{pm} + L_{mf}i_f\right)\omega\cos\theta_i = 0 \tag{14}$$

It is obvious that when the copper loss of field winding and the copper loss of armature winding are equal, the maximum efficiency can be achieved as expressed by (15).

$$R_f i_f^2 = \frac{3}{2} R_s I^2 . \qquad (15)$$

According to (15), the optimal field excitation current can be determined as a function of the winding resistance ratio (R_s / R_f) and the armature current. Both the armature winding and field winding of the prototype machine are located on the same place of the stator, the temperature rises of two windings are assumed to be identical. Furthermore, the same type of coils is used for both the armature winding and the field winding of the prototype machine. Therefore, the winding resistances can be easily replaced by their turn numbers. Since the turn ratio of the prototype machine is 1/3 $(N_s = 184, N_f = 552)$, where N_s and N_f are the turns number of armature winding and field winding respectively, the optimal field excitation current with respect to the maximum efficiency condition can be obtained by (8).

$$i_{f,opt} = \sqrt{\frac{3}{2}\left(\frac{N_s}{N_f}\right)} I = \frac{I}{\sqrt{2}} = \sqrt{\frac{i_d^2 + i_q^2}{2}} \qquad (8)$$

The diagram of the Method-III is shown in Fig. 6. It can be seen from Fig. 6 that the optimal field excitation reference current is employed as shown in (8) to achieve maximum efficiency for the HEDSSM. In the flux-weakening region, both the field excitation and the d-axis currents are utilized to weaken the flux-linkage. Meanwhile, the q-axis current is controlled with regard to the requirement of the speed and load-torque. It should be noted that, the modification of both d-axis and q-axis currents are based on the same principle of Method-II, while the requirements of the d-axis and q-axis currents are reduced compared with the Method-II. Since the calculation of optimal field excitation current requires only the d-axis and q-axis currents, Method-III is easy to implement and robust to the machine parameter variation. The current references of the optimal flux-weakening control method are given in Table III.

TABLE III
OPERATING CONDITIONS OF UTILIZING OPTIMAL METHOD.

REFERENCE CURRENTS	Constant-torque region	Flux-weakening region
i_{dm}^*	0	$i_d^* - \Delta_d$
i_{qm}^*	$\min\left(i_q^*, I_m\right)$	$\min\left(i_q^*, \sqrt{I_m^2 - i_d^2}\right) + \Delta_q$
i_f^*	$i_{f,opt} = \sqrt{\dfrac{i_d^2 + i_q^2}{2}}$	

Fig.6. Optimal flux-weakening control strategy (Method-III).

III. EXPERIMENTAL VERIFICATION OF FLUX-WEAKENING CONTROL STRATEGIES

A. Experimental Setup

The field orientation control algorithm is implemented on a dSPACE platform in order to verify the performance of the proposed methods experimentally. A 1.5 kW wound field type DC machine with the rated speed 1,600 rpm, is utilized to adjust the load-torque, with an external resistance load to dissipate the generated power. The test rig is shown in Fig. 7. In order to increase the utilization of dc-link voltage in flux-weakening region [9], the minimum magnitude error over-modulation (MMEOM) is applied. It is based on the SVPWM switching technique operating with the three-phase voltage source inverter. The field excitation current is regulated by the step-down (buck-type) DC-DC converter. Other setup parameters are defined in Table IV.

Three types of control methods are implemented and compared:

(1) Flux-weakening control method utilizing field excitation current (Method-I);

(2) Flux-weakening control method utilizing armature current (Method-II);

(3) Optimization Method: Flux-weakening control method utilizing both field excitation current and armature current (Method-III).

Fig. 7. Experimental rig.

Maximum armature current	7.92 A
Maximum field excitation current	5.6 A
DC-link voltage	40 V
DC supply voltage of the converter	30V
Switching frequency of the inverter	10kHz
Switching frequency of the converter	10kHz
Maximum motor test speed	1200 rpm
Permanent magnet flux (ψ_{pm})	0.98 mWb
Rated torque	0.71 Nm
Armature winding resistance (R_s)	1 Ω
Field winding resistance (R_f)	3 Ω
d-axis and q-axis inductances (L_d, L_q)	2 mH
Self-inductance of field winding (L_f)	0.5 mH
Number of pole pairs (P)	10
Number of turns per phase of armature winding (N_s)	184
Number of turns of field winding (N_f)	552
Stator outer diameter	90 mm
Axial length	25 mm
Split ratio of stator inner to outer diameter	0.5
Air-gap length	0.5 mm
Stator back-iron thickness	2.0 mm

B. Experimental Results

Fig. 8 shows the measured results of all flux-weakening control methods from 0 to 1200 rpm. The measured torque and output power against speed are shown in Figs. 8(a) and (b), respectively. It is obvious that all control methods can achieve the same torque and output power in the constant-torque region due to the same enhanced field excitation currents as can be seen in Fig. 8(c). In the flux-weakening region, the torque and output power of Method-I is significantly deteriorated and the operating speed range is also limited as only the field excitation current is utilized for flux-weakening control. Meanwhile, in Method-II and Method-III, although the q-axis currents are reduced compared to Method-I, higher torque and power can be obtained in Method-II and Method-III since much higher value of field excitation current can be employed. It is obvious from Figs. 8(c)-(d) that Method-II utilizes only the d-axis current to weaken the flux-linkage, and the field excitation current maintains at its maximum value (5.6 A) in all operating regions. Method-III utilizes both field excitation and d-axis currents to weaken the flux-linkage, Figs. 8(c)-(d). Compared to Method-II, the requirement of the d-axis current is decreased in Method-III. Consequently, higher q-axis current can be utilized under the current-limit as shown in Fig. 8(d).

Fig. 9 shows the measured copper loss and efficiency of all flux-weakening control methods from 0 to 1200 rpm. Method-I exhibits the lowest copper loss of field winding, as shown in Fig. 9(a). In Method-II, the field winding copper loss is kept at 94 W throughout the operating regions, while it can be greatly reduced in the flux-weakening region for Method-III as a result of the optimal field excitation and d-axis armature currents as illustrated in Fig. 8(c). Likewise, the armature winding copper loss of all flux-weakening control methods are shown in Fig. 9(b). These are calculated based on the employment of d-axis and q-axis currents as shown in Fig. 8(d). As a result, the total copper losses for all operating regions which consist of the field winding and the

armature winding copper losses are depicted in Fig. 9(c). It is clear that although the total copper losses of Method-I can be remarkably reduced in the flux-weakening region than Method-II and Method-III, the operating speed range is limited. The power factors for all methods are shown in Fig.9 (d), which are calculated based on the measured voltages and currents. It can be seen from Fig. 9(d) that the power factor for all methods are relatively low, especially in the flux-weakening region due to the high machine speed and modified armature currents. Based on the utilization of the optimal field excitation and d-axis armature currents, Method-III can obtain wider speed region compared to Method-I, and achieve higher efficiency in flux-weakening region compared to Method-II, as shown in Fig. 9(e).
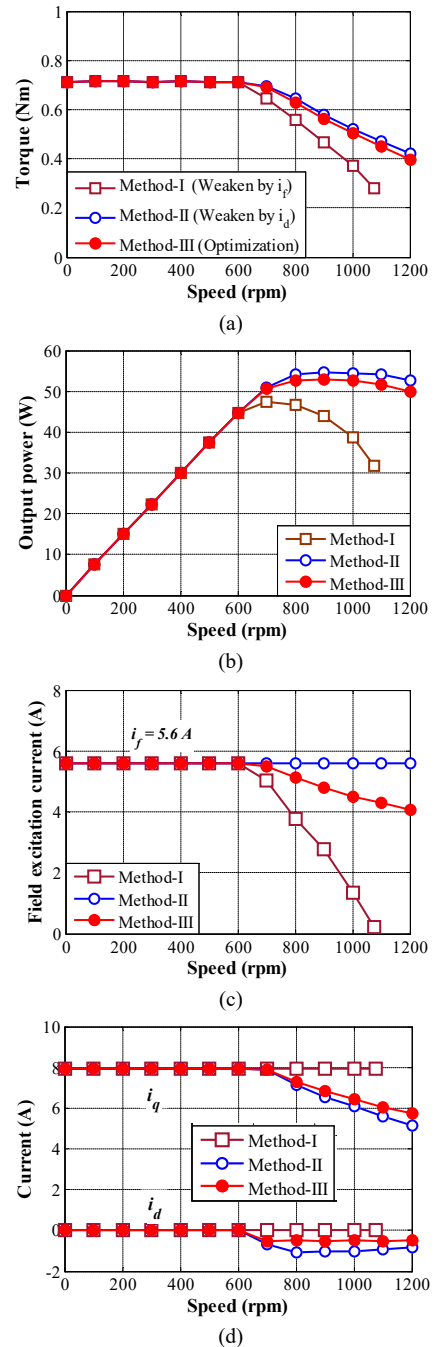

(a)

(b)

(c)

(d)

Fig. 8. Measured results against speed. (a) Torque. (b) Mechanical output power. (c) Field excitation current. (d) d-axis and q-axis currents.
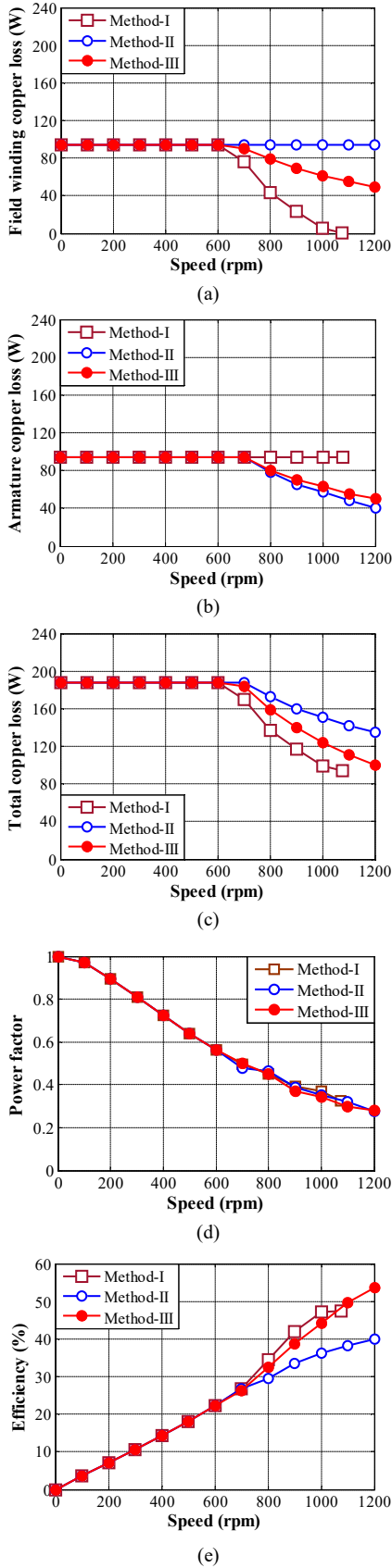
(a)

(b)

(c)

(d)

(e)

Fig. 9. Copper losses, power factor, and efficiency against speed. (a) Field winding copper loss. (b) Armature winding copper loss. (c) Total copper loss. (d) Power factor. (e) Efficiency.

Fig. 10 shows the dynamic response of Method-III. A unit step from 0 to 1000 rpm is set at the instant of 1.0 second, Fig. 10(a). After around 5.0 seconds, the speed can track with its reference. The dynamic response of the optimal field excitation current, the d-axis current, and the q-axis current

are shown in Fig. 10(b). It is obvious that the optimal field excitation current is calculated as the same value as the maximum field exitation current in the constant-torque region corresponding to the results under steady-state condition, Fig. 8(c), and it is gradually modified following the d-axis and q-axis currents in flux-weakening region. In Fig. 10(c), the tracking error minimization of copper losses in both field and armature windings can be achieved. The copper losses in two windings are similar in all operating regions, which is consistent to the principle of Method-III. The total copper loss in Method-III can be considerably reduced in the flux-weakening region compared to Method-II, as shown in Fig. 10(d). Note that since Method-I exhibits low torque in flux-weakening region and the operating speed range is visibly constrained, it will not be reported in the dynamic response.

It also should be noted that the flux-linkage of the HESSDM can be adjusted by field current only, d-axis armature current only, or both of the field current and d-axis armature current. Hence, the maximum achievable constant power speed range (CPSR) of three methods depend on the employed weakening current limit. For example, the maximum speed range of Method-I is around 1175 rpm, as shown in Fig.8(b), where the field excitation current is controlled to zero. It should be noted that for Method-II and III, the maximum achievable CPSR are not shown in the paper, but the speed range can be extended until either field current or d-axis armature current reaches zero.

Among these three methods, Method-III could provide the most extended speed range, since this method utilizes both of field current and armature current to weaken the flux-linkage.

(a)

(b)
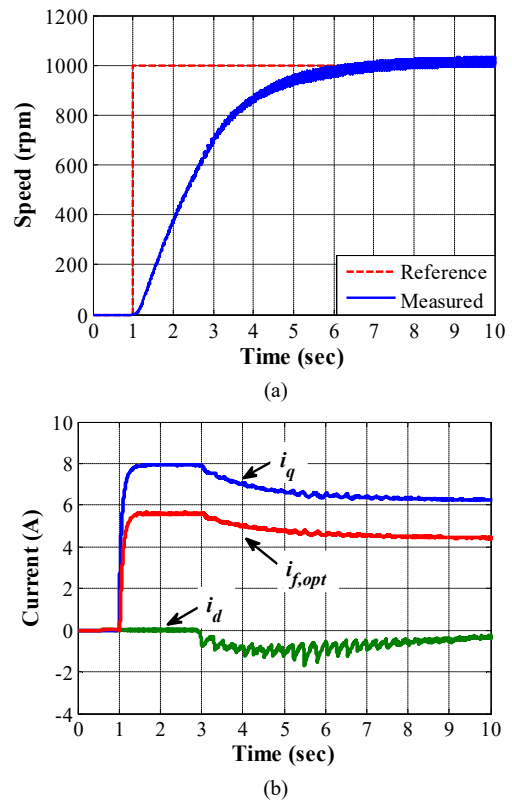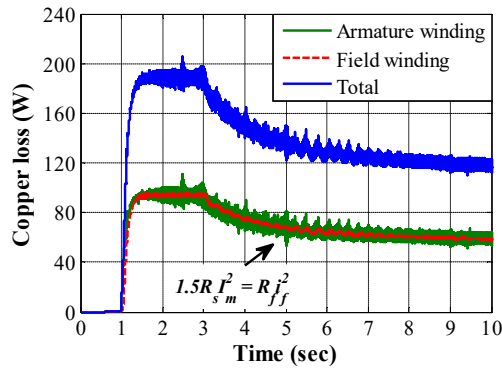
(c)
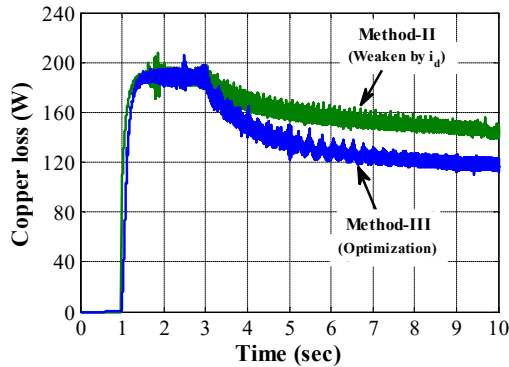
(d)

Fig. 10. Dynamic responses of the Method-III. (a) Speed. (b) *d*-axis current, *q*-axis current, and optimal field excitation current. (c) Tracking error minimization of copper loss. (d) Copper losses.

It should be emphasized that since the prototype machine is a low power machine and the power consumption of field winding is considered, the efficiency is low as shown in Fig. 9. Moreover, a low DC-link voltage is applied in order to limit the testing speed range which is constrained by the test rig. Nevertheless, Method-III has already demonstrated its effectiveness in terms of extending the operating speed range and efficiency improvement in flux-weakening region.

IV. CONCLUSION

Three practical flux-weakening control strategies for the HEDSSMs have been presented in this paper. Those methods can be categorized based on the utilization of weakening currents: (1) Utilizing field excitation current only, (2) Utilizing armature current only, (3) Optimization method which utilizes both the field excitation current and armature current. Based on the experimental results, the optimization method exhibits a wider operating speed range than the method utilizing field excitation current alone and higher efficiency in flux-weakening region than the method-II utilizing armature current only. Furthermore, the optimization method is easy to implement and robust to the variation of machine parameters. It can be easily applied to other hybrid-excited machines as well.

V. REFERENCES

[1] C. D. Nguyen and W. Hofmann, "Self-tuning adaptive copper-losses minimization control of externally excited synchronous motors," *Int. Conf. Electrical Machine (ICEM)*, 2014, pp. 897–902.

[2] Z. Q. Zhu and L. M. Gong, "Improved sensorless operation of permanent magnet brushless ac motors based on online optimal efficiency control," *in Proc. IEEE Int. Elect. Mach. Drive. Conf., Niagara Falls*, Canada, May 15-18, 2011, pp. 1591-1596.

[3] R. Ni, D. Xu, G. Wang, L. Ding, G. Zhang and L. Qu, "Maximum Efficiency Per Ampere Control of Permanent-Magnet Synchronous Machines," *IEEE Trans. Ind. Electron.*, vol. 62, no.4, pp. 2135-2143, April 2015.

[4] I. A. A. Afinowi, Z. Q. Zhu, Y. Guan, J. C. Mipo, and P. Farah, "Hybrid-excited doubly salient synchronous machine with permanent magnets between adjacent salient stator poles," *IEEE Trans. Magn.*, vol. 51, no. 10, pp.1-9, Oct. 2015.

[5] J. T. Chen, Z. Q. Zhu, S. Iwasaki, and R. Deodhar, "A novel hybrid-excited switched-flux brushless AC machine for EV/HEV applications," *IEEE Trans. Veh. Technol.*, vol. 60, no. 4, pp. 1365-1373, May. 2011.

[6] Y. Liu, Z. Zhang, and X. Zhang, "Design and optimization of hybrid excitation synchronous machines with magnetic shunting rotor for electric vehicle traction applications," *IEEE Trans. Ind. Appl.*, vol. 53, no. 6, pp. 5252-5261, Nov./Dec. 2017.

[7] Q. Wang, S. Niu, and X. Luo, "A novel hybrid dual-PM machine excited by AC with DC bias for electric vehicle propulsion," *IEEE Trans. Ind. Electron.*, vol. 64, no. 9, pp. 6908-6919, Sept. 2017.

[8] Z. Q. Zhu, I. A. A. Afinowi, Y. Guan, J. C. Mipo, and P. Farah, "Hybrid-excited stator slot permanent magnet machines-influence of stator and rotor pole combinations," *IEEE Trans. Magn.*, vol. 52, no. 2, pp. 1-10, Feb. 2016.

[9] R. L. Owen, Z. Q. Zhu, and G. W. Jewell, "Hybrid-excited flux-switching permanent-magnet machines with iron flux bridges," *IEEE Trans. Magn.*, vol. 46, no. 6, pp. 1726-1729, Jun. 2010.

[10] Y. Amara, L. Vido, M. Gabsi, E. Hoang, A. H. Ben Ahmed, and M. Lecrivain, "Hybrid excitation synchronous machines: energy-efficient solution for vehicles propulsion," *IEEE Trans. Veh. Technol.*, vol. 58, no. 5, pp. 2137-2149, Jun. 2009.

[11] N. Pothi, Z. Q. Zhu, and Y. Ren, "flux-weakening control of novel hybrid-excited doubly salient synchronous machine", International Conference on Electrical Machines *(ICEM 2018), Alexandroupoli, Greece*, 3-6 Sept. 2018.

[12] N. Pothi and Z. Q. Zhu, "A new control strategy for hybrid-excited switched-flux permanent magnet machines without the requirement of machine parameters," in *Proc. 7th IET Int. Conf. Power Electron., Mach. Drives (PEMD)*, Apr. 2014, pp. 1-6.

[13] S. Shinnaka and T. Sagawa, "New optimal current control methods for energy-efficient and wide speed-range operation of hybrid-field synchronous motor," *IEEE Trans. Ind. Electron.*, vol. 54, no. 5, pp. 2443-2450, Oct. 2007.

[14] M. Huang, H. Lin, H. Yunkai, P. Jin, and Y. K. Guo, "Fuzzy control for flux weakening of hybrid exciting synchronous motor base on particle swarm optimization algorithm," *IEEE Trans. Magn.*, vol. 48, no. 11, pp. 2989–2992, Nov. 2012.

[15] R. Mbayed, G. Salloum, L. Vido, E. Monmasson, and M. Gabsi, "Hybrid excitation synchronous machine control in electric vehicle application with copper losses minimization," in *Proc. 6th IET Int. Conf. Power Electron., Mach. Drives (PEMD)*, Mar. 2012, pp. 1-6.

[16] N. Pothi, Z. Q. Zhu, I. A. A. Afinowi, B. Lee, and Y. Ren, "Control strategy for hybrid-excited switched-flux permanent magnet machines," *IET Electr. Appl.*, vol. 9, no. 9, pp. 612–619, 2015.

[17] T. S. Kwon and S. K. Sul, "A Novel Fux Weakening Algorithm for Surface Mounted Permanent Magnet Synchronous Machines with Infinite Constant Power Speed Ratio," in *Proc. Int. Conf. Elect. Mach. Systems*, Oct. 2007, pp. 440-445.

[18] H. Liu, Z. Q. Zhu, E. Mohamed, Y. Fu, and X. Qi, "Flux-weakening control of nonsalient pole PMSM having winding inductance, accounting for resistive voltage drop and inverter nonlinearities," *IEEE Trans. Power Electron.*, vol. 27, no. 2, pp. 942-952, Feb. 2012.

[19] T. S. Kwon and S. K. Sul, "Novel Antiwindup of a Current Regulator of a Surface-Mounted Permanent-Magnet Motor for Flux-Weakening Control," *IEEE Trans. Ind. Appl.*, vol. 42, No. 5, pp. 1293-1300, Sep./Oct. 2006.

Nattapong Pothi received the B.Eng. and M.Eng. degrees in electrical engineering from Chiang Mai University, Chiang Mai, Thailand, in 2002 and 2006, respectively, and the PhD degree in 2016 from the University of Sheffield, Sheffield, U.K. He is currently lecturing at School of Engineering, University of Phayao, Phayao, Thailand. His research interests are in the areas of electric drives, energy conversion systems, and power electronic applications.

Z.Q. Zhu (F'09) received the B.Eng. and M.Sc. degrees in electrical engineering from Zhejiang University, Hangzhou, China, in 1982 and 1984, respectively, and the Ph.D. degree in electrical engineering from the University of Sheffield, Sheffield, U.K., in 1991. Since 1988, he has been with the University of Sheffield, where he is currently the

Royal Academy of Engineering/Siemens Research Chair and is the Head of the Electrical Machines and Drives Research Group, the Academic Director of Sheffield Siemens Wind Power Research Centre, the Director of Midea Electrical Machines and Controls Research Centre, and the Director of the CRRC Electric Drives Technology Research Centre. His current major research interests include the design and control of permanent-magnet brushless machines and drives for applications ranging from automotive to renewable energy.
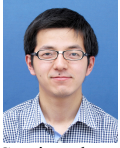
Yuan Ren (M'17) received the B.Eng. and M.Sc. degrees in electrical and electronic engineering from Zhejiang University, Hangzhou, China, in 2009 and 2012, respectively, and the Ph.D. degree in electrical engineering from the University of Sheffield, Sheffield, U.K., in 2016. Since 2016, he has been a KTP Associate between Dynex Semiconductor, Ltd., Lincoln, U.K., and the University of Sheffield. His research interests include power devices, electrical machines, and control strategies for electric vehicles.